LANGMUIR

Article pubs.acs.org/Langmuir

Printable Organic Electronic Materials for Precisely Positioned Cell **Attachment**

Jeffrey A. Horowitz, Xiaoyang Zhong, Samuel J. DePalma, Maria R. Ward Rashidi, Brendon M. Baker, Joerg Lahann, and Stephen R. Forrest*



Cite This: Langmuir 2021, 37, 1874-1881



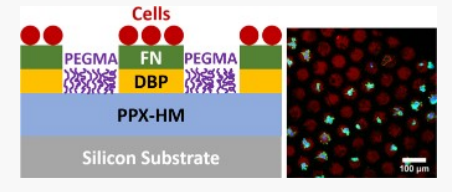
ACCESS |

III Metrics & More

Article Recommendations

Supporting Information

ABSTRACT: Over the past 3 decades, there has been a vast expansion of research in both tissue engineering and organic electronics. Although the two fields have interacted little, the materials and fabrication technologies which have accompanied the rise of organic electronics offer the potential for innovation and translation if appropriately adapted to pattern biological materials for tissue engineering. In this work, we use two organic electronic materials as adhesion points on a biocompatible poly(p-xylylene) surface. The organic electronic materials are precisely deposited via vacuum thermal



evaporation and organic vapor jet printing, the proven, scalable processes used in the manufacture of organic electronic devices. The small molecular-weight organics prevent the subsequent growth of antifouling polyethylene glycol methacrylate polymer brushes that grow within the interstices between the molecular patches, rendering these background areas both protein and cell resistant. Last, fibronectin attaches to the molecular patches, allowing for the selective adhesion of fibroblasts. The process is simple, reproducible, and promotes a high yield of cell attachment to the targeted sites, demonstrating that biocompatible organic small-molecule materials can pattern cells at the microscale, utilizing techniques widely used in electronic device fabrication.

1. INTRODUCTION

Researchers have engineered cell-surface interactions since the 1960s, 1,2 but with advances in cell patterning, 3 microstructured stem cells have inspired the promise of developing human tissue in vitro. The differentiation and survival of stem cells are highly dependent on their microenvironment, in particular, the interactions between cells and extracellular matrices (ECMs).⁴ The size of adhesion points⁵ and the spatial distribution and alignment of stem cells have been shown to significantly impact stem cell behavior.^{6,7} Therefore, much attention has been given to the precise positioning of cells onto scaffolds in vitro. Many techniques of attachment site patterning have been developed, including but not limited to microcontact printing, 5,8-10 stencil-based patterning, 11,12 photolithography- and photografting-based methods, 13-18 as well as approaches utilizing click chemistry 19 or surface acoustic waves.²⁰

In two dimensions, cells can be precisely positioned using antifouling materials to mediate the surface interactions of ECM proteins.¹² Nonfouling surfaces are often patterned to ensure spatially controlled decoration of substrates with ECM proteins such as fibronectin, collagen, or laminin. For example, microcontact printing can be used to directly transfer the ECM proteins or to transfer other materials, changing local surface characteristics.^{3,21} Photolithography takes advantage of the photoactive properties of materials, including their tendencies to polymerize, cross-link, or degrade under illumination. Local adhesion regions can therefore be formed through the photopatterning of hydrogels, ¹³ polymer brushes, ¹⁴ or proteins themselves.²² Polyethylene glycol (PEG)-based compounds, often considered biologically inert as they do not mediate interactions with most proteins, 23,24 are a popular choice for preventing the attachment of ECM adhesion proteins.

In this work, we introduce a new process whereby patterning is performed by the gas-phase deposition of organic electronic materials using chemical vapor deposition (CVD), vacuum thermal evaporation (VTE), and organic vapor jet printing (OVJP). This is motivated by the successful use of such materials and methods in the high-volume manufacture of organic electronic devices, such as organic light-emitting diode displays and solar cells, over very large areas.²⁵ Adaptation of such methods to tissue engineering provides a unique opportunity for the rapid, large-scale production of tissues for therapeutic and experimental protocols. The process uses biocompatible, printable organic electronic materials as adhesion points, deposited onto a poly(hydroxymethyl-pxylylene) (PPX-HM) surface which is readily deposited using CVD polymerization. Following an initiator reaction, antifouling polyethylene glycol methacrylate (PEGMA) polymer brushes are selectively grown in the spaces between adhesion points. Fibronectin attaches only to the adhesion points,

Received: November 17, 2020 Revised: January 12, 2021 Published: January 26, 2021





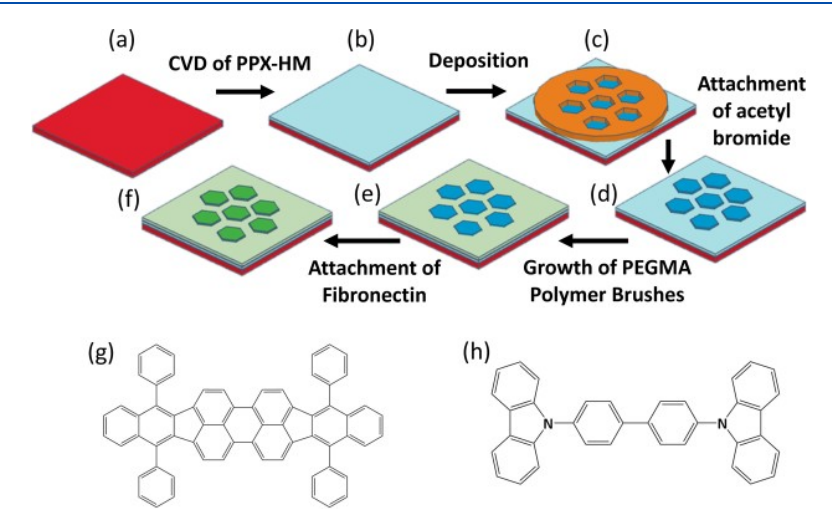


Figure 1. Cell patterning process flow. (a) Si substrate is coated with (b) PPX-HM by CVD. (c) PDMS holds a TEM grid onto the substrate as a mask and an organic small-molecule material (DBP or CBP) is deposited through the mask by VTE onto the PPX-HM surface. This step may be replaced by direct patterning *via* OVJP. (d) Initiator reaction in a vacuum desiccator forms acetyl bromide on the hydroxymethyl group of PPX-HM. (e) PEGMA polymer brushes are grown from acetyl bromide by an atomic transfer radical polymerization reaction in solution. (f) Fibronectin is deposited, only attaching to the regions without PEGMA polymer brushes. Molecular structural formulae of (g) DBP and (h) CBP.

enabling the selective attachment of murine fibroblasts (NIH3T3). The material choice for adhesion points proves important, not only for its effect on fibronectin but also for its biocompatibility and ability to withstand solution-processed growth of PEGMA without delamination.

Although organic semiconductor materials are patterned at the micron scale for OLED displays, their gas-phase deposition has not yet been considered for the precise patterning of cells. The primary objectives of this work are to (i) demonstrate the viability of nontoxic small-molecule organic semiconductors for patterning cells, (ii) demonstrate that multiple deposition techniques and materials may be used to effectively perform this function, and (iii) present these as useful alternatives to conventional patterning methods. Here, the common organic electronic materials^{26–29} tetraphenyldibenzoperiflanthene (DBP) and 4,4'-bis(carbazole-9-yl)biphenyl (CBP) are deposited as adhesion points. These materials are chosen because they have relatively different chemical compositions and structures and different physical properties in thin films. Additionally, both materials are well known as useful for organic electronics^{26,29,30} and therefore already well understood. However, DBP and CBP are by no means uniquely suitable for cell attachment-they are only representative of a very wide range of organic semiconductors from which to choose, thus pointing to the enormous versatility offered by our approach.

2. EXPERIMENTAL SECTION

2.1. Cell Patterning Procedures. Figure 1 provides a diagram of the patterning process based on the VTE of attachment points. Silicon substrates (1 cm²) are sequentially cleaned with 1:100 Tergitol in deionized (DI) water, acetone, isopropanol, and ultraviolet-ozone plasma (Figure 1a). Next, a layer of PPX-HM is grown by CVD using the Gorham process (Figure 1b). 31,32 The PPX-HM precursor is homolytically cleaved in a furnace with zones set at 450, 550, and 560 °C. The substrate is kept at 15 °C during deposition, allowing the reactive pyrolysis products to polymerize on its surface. The CVD system 33 is pumped to 8 mtorr and then purged with 20 standard cubic centimeters per minute (SCCM) of Ar, resulting in a pressure of 0.08 torr. The deposition is at a rate of 0.1 Å/s, resulting in a 15–20 nm thick layer of PPX-HM, as measured by ellipsometry. Supporting

Information Figure S1 describes the polymerization process of PPX-HM

Organic electronic small-molecule adhesion points are formed on the PPX-HM surface either by VTE through a mask (Figure 1c) or by direct, high-speed printing by OVJP. For VTE, a biopsy punch is used to form a 2.5 mm radius hole in a 1–3 cm thick layer of polydimethylsiloxane (PDMS) with an area of 1 cm². Transmission electron microscopy (TEM) grids are placed over these holes as deposition masks. The masks are attached to the substrates which are then placed in a vacuum chamber (base pressure < 10^{-6} torr), followed by thermal evaporation of a 20 nm thick layer of DBP or CBP. All small-molecule materials along with the parylene precursors were purchased from commercial vendors. After deposition, the PDMS and TEM grids are removed leaving hexagonal patterns.

Organic vapor jet printing of the small-molecule attachment points employs a custom printing apparatus described elsewhere $^{34-36}$ (also see Figure S2). Briefly, small molecular-weight organic material is evaporated into a hot N_2 gas stream at a flow rate of 2 standard cubic centimeters per minute that entrains the volatilized material through microfluidic channels to a silicon micronozzle array heated to 200 °C. The nozzles are brought within 100 μ m of the cooled substrate to enable local adsorption of the volatilized species. This allows for small ($\sim 1-10~\mu$ m) features to be printed at rapid rates (many cm/s). 34 In this work, PPX-HM-coated substrates are placed in a vacuum chamber at a pressure of 0.08 torr on a substrate holder which is mounted on a translation stage and cooled to 5 °C. The substrate is translated at 7 mm/s to deposit lines of material. The thickness of lines changes with the angle between the rectangular nozzle outlet (Figure S2c) and the direction of translation.

Following vapor phase deposition and patterning, samples are placed in a vacuum desiccator with four glass slides. Triethylamine is placed on each of two glass slides and 2-bromoisobutyryl bromide (30 μ L on each glass slide) on the other two. The reaction, occurring overnight (approximately 18 h), attaches 2-bromoisobutyryl onto the hydroxymethyl group of PPX-HM (Figure 1d). 2-bromoisobutyryl does not form on regions of PPX-HM covered by deposited organic electronic material. PEGMA polymer brushes are then grown via an atom transfer radical polymerization (ATRP) reaction where a mixture of 4 g of PEGMA, 7 mg of CuBr₂, and 20 mg of CuBr, in 10 mL of DI water is reacted with 30 mg of 2,2'-bipyridyl in 10 mL of DI water. The reaction occurs over 90 min, growing PEGMA polymer brushes to a height of 20–30 nm off of the acetyl bromide groups on PPX-HM (Figure 1e). The reaction occurs over 90 min, growing PEGMA polymer brushes to a height of 20–30 nm off of the acetyl bromide groups on PPX-HM (Figure 1e). The reaction occurs over 90 min, growing PEGMA polymer brushes to a height of 20–30 nm off of the acetyl bromide groups on PPX-HM (Figure 1e). The reaction occurs over 90 min, growing PEGMA polymer brushes to a height of 20–30 nm off of the acetyl bromide groups on PPX-HM (Figure 1e).

Fourier transform infrared spectroscopy (FTIR) spectra of the PEGMA brush growth process are provided in Figure S3.

Alexa Fluor 555-labeled fibronectin or unlabeled fibronectin is coated onto the samples at a concentration of 50 $\mu g/mL$ in prebuffered saline (PBS) solution (Figure 1f). The fibronectin-coated samples are incubated for 1 h and rinsed to remove excess solution. Murine fibroblasts (NIH3T3) are cultured at 37 °C and 5% CO₂ in Dulbecco's Modified Eagle Medium (DMEM) containing 1% penicillin/streptomycin, L-glutamine, and 10% bovine serum. The culture media is aspirated, and substrates are rinsed twice with PBS, followed by the addition of 0.5 mL of 0.05% trypsin-EDTA (ethylenediamine tetra-acetic acid). The cultures are incubated at 37 °C for 5 min, causing the cells to detach from the surface. Trypsin is deactivated by adding 1.5 mL of culture media to each well, and the cell solution is transferred to a 15 mL tube. Cells are seeded at a density of 12,000 or 10,000/cm² and incubated overnight, after which they are fixed in 4% paraformaldehyde for 10 min and rinsed twice with PBS. The samples are treated with 4',6-diamidino-2-phenylindole (DAPI) to image nuclei blue and with Alexa Fluor 488-labeled phalloidin to image F-actin. All fluorescent images are taken with a laser scanning confocal microscope (Zeiss LSM800). Molecular structural formulae of DBP and CBP, the two organic semiconductors, are given in Figure 1g,h, respectively.

- **2.2. Confocal Imaging.** Silicon substrates with patterned cells and fibronectin are placed on glass microscope slides, with the patterned surface facing the glass. The microscope slides are flipped and placed in the Zeiss LSM800 confocal microscope such that the patterned surface faces the laser and lens to image the sample surface. The laser wavelengths used are 405 nm to image DAPI, 488 nm to image Alexa Fluor 488, and 555 nm to image Alexa Fluor 555.
- **2.3. Spectroscopic Sample Preparation.** XPS measurements were performed with a monochromatic Kratos Axis Ultra X-ray photoelectron spectrometer on 20 nm thick small-molecule films and PPX-HM deposited onto cleaned Si substrates. The Al X-ray gun emission current was 8 mA with a 14 kV high-temperature anode in a sample-analysis chamber at 10⁻⁸ torr. Sample charging was corrected assuming 284.8 eV as C 1s binding energy. Fourier transform infrared (FTIR) spectrometry measurements were performed using a Thermo Nicolet 6700 spectrometer with a grazing angle accessory on a 20 nm thick film of PPX-HM deposited onto cleaned Au substrates.
- **2.4. Biocompatibility Testing.** The biocompatibility of organic small-molecule materials is determined using 20 nm thick, neat layers of vacuum-deposited DBP and CBP. Cells are cultured and seeded as described above, incubated overnight, and rinsed with PBS. Calcein acetoxymethyl (Calcein AM) is added, exhibiting green fluorescence within living cells, and ethidium homodimer-1 is added to stain the dead cells red. The combined solution (100–150 μ L) is added, and the cells are incubated for 30–45 min at room temperature. Images are acquired using a laser scanning confocal microscope as above.

3. RESULTS

In Figure 2a, the red fluorescence of DBP indicates the vacuum-deposited pattern. Cell nuclei and F-actin, visible in blue and green, respectively, are centered almost entirely on the target regions. Because of the strong red fluorescence of DBP and limited available laser lines for imaging, fibronectin is stained green and imaged on separate samples (Figure 2b). Fibronectin also shows considerable adhesive selectivity, with the hexagon array clearly visible. The DBP adhesion points are stable during solution processing used for the growth of the polymer brushes. As a nonpolar hydrocarbon, DBP is insoluble in DI water, while its nearly planar structure promotes strong van der Waals bonding to the PPX-HM surface.²⁶ DBP therefore provides an effective surface for the subsequent attachment of fibronectin and cells. Nonselective areas show fluorescence between the hexagons where DBP, because of a lack of contact between the deposition mask and the substrate, has been inadvertently deposited underneath the shadow mask

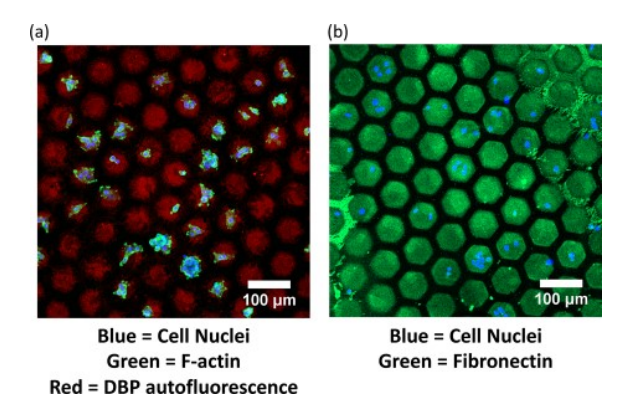
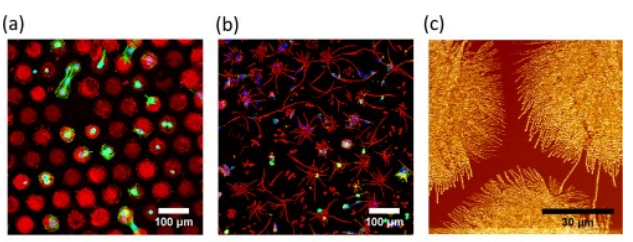


Figure 2. Cells and fibronectin positioned on hexagonal arrays of vacuum-deposited DBP. (a) DBP-patterned substrates with fibronectin and murine fibroblasts attached. In this image, red indicates the fluorescence of DBP, green F-actin, and blue the cell nuclei with fibronectin unlabeled. Cells are seeded at a density of 12,000/cm². (b) DBP-patterned substrates with green-stained fibronectin. Cells are seeded at a density of 10,000/cm².

grid lines visible in the top-right and bottom-left corners of Figure 2b. The growth of PEGMA brushes is thus inhibited in these regions, and consequently, fibronectin or cells may attach between the target regions.

CBP-patterned samples (Figure 3a,b) also display the selective attachment of fibronectin and fibroblasts, although

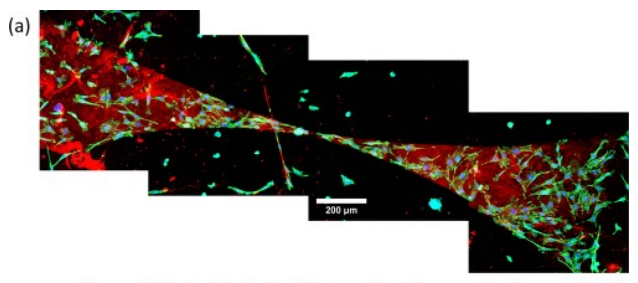


Blue = Cell Nuclei, Red = Fibronectin, Green = F-actin

Figure 3. Cells and fibronectin positioned on hexagonal arrays of vacuum-deposited CBP. (a) CBP-patterned sample with cell nuclei, fibronectin, and F-actin centered on a hexagonal array of adhesion regions. (b) CBP-patterned sample with fibronectin considerably affected by the surface properties of CBP, forming a dendrite-like pattern repelled away from the hexagon region. (c) Atomic force microscopy image of CBP-patterned samples after the growth of PEGMA polymer brushes, showing considerable surface roughness and crystallinity.

with lower selectivity than DBP. This is due to CBP's tendency to aggregate into polycrystals³⁸ on the PPX-HM surface. The loosely adhered aggregates may delaminate during polymer brush growth, leaving behind a rough surface, apparent in the atomic force microscope image in Figure 3c. The surface roughness is especially noticeable in Figure 3b where fibronectin assumes dendrite-like features. Note that CBP is a nonpolar molecule insoluble in water. However, aggregates can be lifted off by solvent exposure if they are not strongly attached to the surface. Despite the irregular surface morphology, fibronectin mostly adheres to CBP, and the cells are predominantly contained within the target regions.

Because of its relatively low vaporization enthalpy,³⁹ CBP is readily printable using OVJP, as shown by the printed pattern decorated with cells in Figure 4a. Sample rotation during deposition produces the apparent bowtie pattern whose



Blue = Cell Nuclei, Red = Fibronectin, Green = F-actin

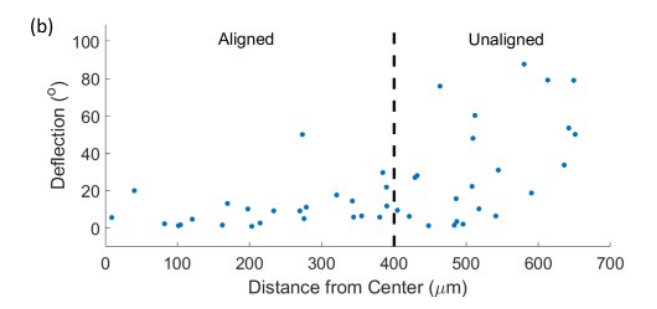


Figure 4. (a) Cells and fibronectin positioned onto a bowtie pattern deposited by OVJP, with fibronectin red, cell nuclei blue, and F-actin green. (b) Deflection from the center axis of the bowtie as a function of distance from the center of the bowtie. Cells generally displayed considerable alignment to the pattern less than 400 μ m from its center, and were unaligned at greater distances. The vertical dashed line indicates a transition from aligned to unaligned.

longitudinal axis is along the direction of the stage motion. This allows for the determination of the dependence of cell alignment on adhesion-region width. Fibronectin (red) indicates the printed pattern, with most of the cells attached to this pattern. F-actin (green) displays alignment in the narrow regions of the pattern and orientational randomness in the wider regions. Axial deflection of the cells from the central axis of the bowtie pattern is plotted in Figure 4b. Approximately 400 μ m from the center of the bowtie, indicated in Figure 4b by the vertical dashed line, the cell alignment along the pattern edges is lost, and the cell deflection angle becomes random. This corresponds to a pattern width of about 110 μ m on the bowtie pattern.

A notable feature of this pattern is that the neck of the bowtie is approximately 10 $\mu \rm m$ wide. Apparently, this region favors a single cell oriented along the pattern axis. This provides a scale as to the minimum practical size of the attachment points. Furthermore, some cells attach outside of the printed pattern. This is attributed to debris and other defects that exist on the substrate, including areas contaminated by over-spray from the nozzle during sample manipulation as apparent from the scattered red luminescence in the black background field. Overspray in OVJP deposition is eliminated by placing the nozzle array closer to the substrate.

Patterning accuracy is defined as the ratio of imaged fluorescence within the target adhesion regions to the fluorescence of the entire image field. MATLAB⁴⁰ is used to generate the target adhesion pattern to label fluorescence as inside or outside the target region. These patterns are visible in red in Figure 5a as a hexagon array and green in Figure 5b as a bowtie for VTE and OVJP samples, respectively. Thus, the patterning accuracies of the CBP-patterned samples of

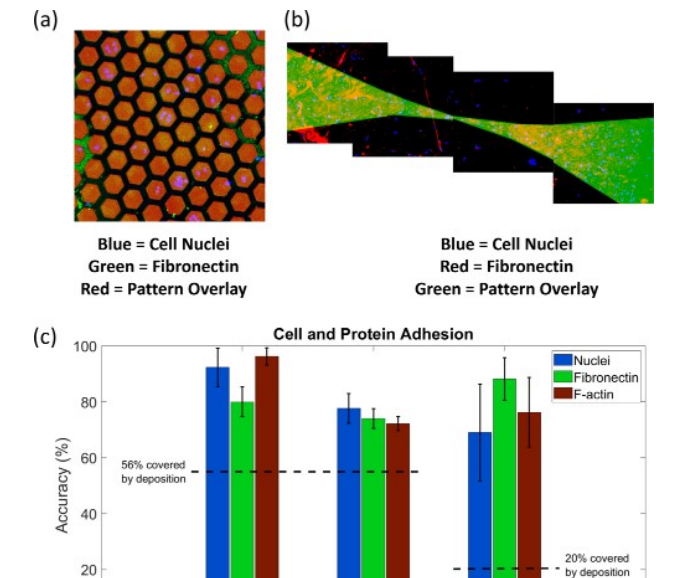


Figure 5. (a) Image of the computer-generated hexagonal lattice (red) overlain on an image to determine the patterning accuracy of samples patterned with VTE. (b) Image of a computer-generated bowtie shape overlain on an image to determine the patterning accuracy of samples patterned with OVJP. (c) Statistical analysis of the patterning accuracies on different materials and with different techniques, showing the nuclei (left bar), fibronectin (middle bar), and F-actin (right bar). Horizontal dashed lines indicate the percentage of the images covered by the deposition.

CBP (Evaporation)

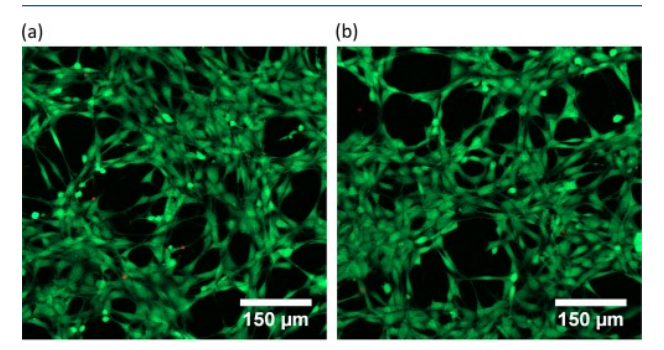
CBP (OVJP)

fibronectin, cell nuclei, and F-actin are found by the ratios of the intensities of red, blue, and green within the target regions to the intensities in the total image. The bright red fluorescence of DBP does not permit imaging other features in red, so patterning accuracy for fibronectin is calculated using green-stained fibronectin, and patterning accuracy for F-actin is calculated on separate samples with unlabeled fibronectin and green-stained phalloidin.

The results of this statistical procedure are provided in Figure 5c. For DBP, an average of $80 \pm 5\%$ of the fibronectin is found within the hexagonal patches, while for CBP, $74 \pm 4\%$ is found within the deposition areas. The value for CBP is slightly lower because the surface grooves due to crystallization apparently repel fibronectin. Cell nuclei are patterned onto DBP with an average yield of 92 \pm 7% and on CBP with an average yield of $78 \pm 5\%$. The discrepancy between the attachment yields of CBP and DBP is again due to the outward-branching fibronectin on the dendritic CBP points. Factin is patterned on DBP with an attachment yield of 96 \pm 3% and CBP with a yield of 72 \pm 3%, closely correlated with the corresponding patterning yields of nuclei. OVJP-patterned samples display attachment yields of 69 \pm 17% for cell nuclei, 88 \pm 8% for fibronectin, and 76 \pm 13% for F-actin. As indicated by the horizontal dashed lines in Figure 5c, the vacuum deposited hexagonal array patterns cover 56% of a given image. OVJP patterns only cover 20% of the images, and therefore the patterning accuracies are skewed lower. As controls, Figure S4 displays fibronectin and cells adhered to neat layers of PEGMA brushes, DBP, and CBP, and Figure S5 displays cells and fibronectin adhered to DBP- and CBP- patterned substrates without the growth of PEGMA polymer brushes. Evidently, PEGMA brushes effectively resist the attachment of fibronectin and cells and allow for the selective patterning demonstrated here.

Previous studies have examined the effects of surface properties on fibronectin and cell attachment. In this work, the size of attachment regions, roughness, and wettability are particularly relevant to explain our results. Hydrophobicity causes fibronectin to bind to surfaces in high densities, 42,43 as the introduction of the protein increases entropy. This is demonstrated in Figure S5, in which the red-stained fibronectin selectively attaches to the non-polar patches of CBP and DBP rather than to the polar PPX-HM regions. Additionally, the dendritic surface of CBP influences cell attachment and spreading. Surface grooves cause an increase in surface area, increasing the density of fibronectin adsorption within the grooves. This is demonstrated in Figure 3b where the fibronectin attaches along the CBP dendritic fibers.

Biocompatibility is assessed for neat films of DBP (Figure 6a) and CBP (Figure 6b), deposited by VTE onto precleaned



Green = Living Cells, Red = Dead Cells

Figure 6. Biocompatibility test of fibroblasts on two vacuum-deposited, organic small-molecule materials, with live cells stained green and dead cells red. Fibroblasts are attached to surfaces coated with (a) DBP and (b) CBP. The lack of red in the images indicates the lack of toxicity experienced by cells contacting these films.

Si substrates. The almost complete viability (green luminescence corresponding to live cells vs red luminescence for dead cells) of the attached cells demonstrates the lack of toxicity of these molecules. Tissue culture plastic was used as a control substrate, demonstrating an average of 99 \pm 1% living cells. DBP and CBP demonstrated 99.1 \pm 0.6% and 98.9 \pm 0.7% living cells, respectively. More extensive analyses of the biocompatibility of organic semiconductors have been performed elsewhere.

4. DISCUSSION

In this work, biocompatible organic electronic materials are vacuum deposited or vapor jet printed to form adhesion regions for the selective patterning of cells. Since the patterning of cells on a micrometer scale has been achieved previously, ^{3,8,49} it is worthwhile to compare these procedures to existing techniques. Additionally, while there are many alternative techniques for patterning cells, ^{18–20} a comprehensive review is beyond the scope of this work. The comparisons are therefore limited to the conventional methods of microcontact printing and photopatterning.

Microcontact printing employs a patterned elastomer stamp that is coated with ink and pressed onto a substrate, transferring its pattern.^{3,8} This technique commonly transfers an adhesive protein such as fibronectin onto a cell-inhibiting surface to which cells are subsequently seeded.²¹ Limitations of the process include pattern deformation⁵⁰ and the necessity for a target substrate to withstand the pressure needed for the transfer. Alternatively, photolithography can be used to directly pattern the substrate. While two-photon lithography has yielded impressive three-dimensional patterning of hydrogels, its throughput is insufficient for use in high volume production. This limitation is avoided in direct photolithographic patterning,⁵¹ although it may require the use of solvents and polymers whose properties are incompatible with those of the target scaffold or substrate.

In contrast, both vacuum-deposition and vapor jet printing are simple, with an immense variety of available molecules developed for the organic electronics industry. Furthermore, the processes avoid chemical degradation or direct contact with the surface. Drawbacks to VTE include the need for deposition masks with their limited spatial resolution and difficulties in printing on 3-dimensional or structured surfaces. On the other hand, direct printing by OVJP eliminates the requirement for deposition masks and provides more flexibility and control in three dimensions since the patterning accuracy is only dependent on the nozzle diameter and its distance from the target surface. 34,35

The main advantage of VTE and OVJP is the scalability and rapidity of pattern formation. This is estimated by assuming a film thickness writing speed of d = Wr/v, where W is the width of the evaporated plume or jet, r is the evaporation rate, and vis the translation velocity of the substrate.⁵² A linear source boat, shown in Figure S6a, allows for the patterning of the entire width of a substrate, or a batch of substrates, in a single pass. Using the VTE parameters in this work, r = 0.5 Å/s and d= 20 nm, and restricting the plume width to W = 5 cm to fully cover the shadow mask and substrate areas, the substrate can be translated at 125 μ m/s, leading to a patterning throughput of 45 cm²/h, although throughput may be increased by simultaneously patterning multiple or larger area substrates. OVJP is capable of significantly higher deposition rates (>80 nm/s), allowing for higher substrate translation speeds. For example, using an OVJP print head with 300 μ m long nozzles, 20 nm thick films can be deposited with a substrate translation speed of 1.2 mm/s. This corresponds to a printing throughput of \sim 430 cm²/h. In this work, substrates were translated at 7 mm/s for OVJP deposition, allowing for even higher throughputs.

5. CONCLUSIONS

We have demonstrated a simple, high-yield, and biocompatible process for the selective attachment of fibroblasts using the vapor-phase deposition of organic small-molecule thin films. The process may be extended into three dimensions by repeating deposition for multiple stacked layers on scaffolds, mimicking three-dimensional tissue. As a direct printing technology, OVJP is especially promising for patterning fibrous networks in three dimensions. Future research may also involve high-throughput implementations, for example in a roll-to-roll system. S5,56 Finally, the electronic properties of organic semiconductors are advantageous for the controlled sensing and stimulation of cells. S7,58

The utilization of vapor-phase deposition has several benefits. Contact with the substrate is not required, and simple additive processes such as described here can be used to define the attachment and inhibiting regions. Both OVJP and VTE are mature, high-throughput technologies currently used in the mass production of organic light-emitting diode displays and organic solar cells. There is also a vast variety of organic small-molecule materials, allowing for the optimization of parameters most suited for particular cell chemistry or scaffold attachment application. The selection of this method for cell patterning ultimately depends on the needs of the application. As many studies demonstrate effects of micron- and submicron-scale surface features on proteins and cells, 59-61 patterning resolution is an important consideration. OVJP has a resolution limit <1.5 μ m, ³⁴ while VTE can achieve submicron-resolution with nanofabricated masks. 62,63 The advantages outlined above—the wide range of already available materials, lack of contact with or degradation of a surface, high pattern resolution, demonstrated use in high-throughput production, and integration with electronics-are relevant for the layer-by-layer construction of three-dimensional patterned networks. The vapor-phase deposition of organic smallmolecule materials by VTE or OVJP can accurately guide cells to targeted locations while leaving a delicate scaffold intact. These methods therefore suggest a future use in patterning cells for tissue engineering.

ASSOCIATED CONTENT

Supporting Information

The Supporting Information is available free of charge at https://pubs.acs.org/doi/10.1021/acs.langmuir.0c03319.

Schematic of PPX-HM polymerization; drawings of the OVJP apparatus and a silicon micronozzle array; spectroscopic analysis of the ATRP reaction for PEGMA polymer brush growth by XPS and FTIR; fibronectin and cells adhered to the neat layers of PEGMA polymer brushes, DBP, and CBP; fibronectin and cells with PEGMA polymer brushes adhered to patterned DBP and CBP; and drawing of VTE from a linear source boat and OVJP (PDF)

AUTHOR INFORMATION

Corresponding Author

Stephen R. Forrest — Department of Electrical and Computer Engineering, University of Michigan, Ann Arbor, Michigan 48109, United States; orcid.org/0000-0003-0131-1903; Email: stevefor@umich.edu

Authors

Jeffrey A. Horowitz — Department of Electrical and Computer Engineering, University of Michigan, Ann Arbor, Michigan 48109, United States

Xiaoyang Zhong — Department of Materials Science and Engineering and Biointerfaces Institute, University of Michigan, Ann Arbor, Michigan 48109, United States

Samuel J. DePalma — Department of Biomedical Engineering, University of Michigan, Ann Arbor, Michigan 48109, United States

Maria R. Ward Rashidi — Department of Materials Science and Engineering and Biointerfaces Institute, University of Michigan, Ann Arbor, Michigan 48109, United States

Brendon M. Baker — Department of Biomedical Engineering, University of Michigan, Ann Arbor, Michigan 48109, United States; orcid.org/0000-0002-2785-1070 Joerg Lahann — Department of Materials Science and Engineering and Biointerfaces Institute, University of Michigan, Ann Arbor, Michigan 48109, United States

Complete contact information is available at: https://pubs.acs.org/10.1021/acs.langmuir.0c03319

Funding

This work is supported by the Engineering Research Centers Program of the National Science Foundation under NSF Cooperative Agreement No. EEC-1647837.

Notes

The authors declare no competing financial interest.

ACKNOWLEDGMENTS

We acknowledge Jeffery Raymond for assistance with image analysis in this work. We also acknowledge the Cellular Metamaterials National Science Foundation Engineering Research Center (NSF-ERC).

ABBREVIATIONS

ECM, extracellular matrix; PEG, polyethylene glycol; PEGMA, polyethylene glycol methacrylate; PPX-HM, poly-(hydroxymethyl-p-xylylene); CVD, chemical vapor deposition; PDMS, polydimethylsiloxane; TEM, transmission electron microscopy; DBP, tetraphenyldibenzoperiflanthene; CBP, 4,4′-bis(N-carbazolyl)biphenyl; XPS, X-ray photoelectron spectroscopy; FTIR, Fourier transform infrared spectroscopy; DAPI, 4′,6-diamidino-2-phenylindole; PBS, pre-buffered saline; DMEM, Dulbecco's modified eagle medium; EDTA, ethylenediamine tetra-acetic acid; OVJP, organic vapor jet printing

■ REFERENCES

- (1) Carter, S. B. Haptotactic Islands: A Method of Confining Single Cells to Study Individual Cell Reactions and Clone Formation. *Exp. Cell Res.* **1967**, *48*, 189–193.
- (2) Hauschka, S. D.; Konigsberg, I. R. The Influence of Collagen on the Development of Muscle Clones. *Proc. Natl. Acad. Sci. U.S.A* **1966**, 55, 119–126.
- (3) Zhang, S.; Yan, L.; Altman, M.; Lässle, M.; Nugent, H.; Frankel, F.; Lauffenburger, D. A.; Whitesides, G. M.; Rich, A. Biological Surface Engineering: A Simple System for Cell Pattern Formation. *Biomaterials* 1999, 20, 1213–1220.
- (4) Discher, D. E.; Mooney, D. J.; Zandstra, P. W. Growth Factors, Matrices, and Forces Combine and Control Stem Cells. *Science* **2009**, 324, 1673–1677.
- (5) Chen, C. S.; Mrksich, M.; Huang, S.; Whitesides, G. M.; Ingber, D. E. Geometric Control of Cell Life and Death. *Science* **1997**, *276*, 1425–1428.
- (6) Kim, J.; Kim, H. N.; Lim, Ki-T.; Kim, Y.; Seonwoo, H.; Park, S. H.; Lim, H. J.; Kim, D.-Ho; Suh, K.-Y.; Choung, P.-H.; Choung, Y.-H.; Chung, J. H. Designing Nanotopographical Density of Extracellular Matrix for Controlled Morphology and Function of Human Mesenchymal Stem Cells. Sci. Rep. 2013, 3, 3552.
- (7) Lim, S. H.; Liu, X. Y.; Song, H.; Yarema, K. J.; Mao, H.-Q. The Effect of Nanofiber-Guided Cell Alignment on the Preferential Differentiation of Neural Stem Cells. *Biomaterials* **2010**, *31*, 9031–9039
- (8) Singhvi, R.; Kumar, A.; Lopez, G.; Stephanopoulos, G.; Wang, D.; Whitesides, G.; Ingber, D. Engineering Cell Shape and Function. *Science* **1994**, 264, 696–698.
- (9) Whitesides, G. M.; Ostuni, E.; Takayama, S.; Jiang, X.; Ingber, D. E. Soft Lithography in Biology and Biochemistry. *Annu. Rev. Biomed. Eng.* **2001**, *3*, 335–373.

- (10) Xia, Y.; Whitesides, G. M. Extending Microcontact Printing as a Microlithographic Technique. *Langmuir* **1997**, *13*, 2059–2067.
- (11) Chandra, P. K.; Soker, S.; Anthony, A.. Tissue Engineering: Current Status and Future Perspectives. In *Principles of Tissue Engineering*; Lanza, R., Langer, R., Vacanti, J., Anthony, A., Eds.; Academic Press, 2020; pp 1–35.
- (12) Guillotin, B.; Guillemot, F. Cell Patterning Technologies for Organotypic Tissue Fabrication. *Trends Biotechnol.* **2011**, *29*, 183–190.
- (13) Hahn, M.; Taite, L.; Moon, J.; Rowland, M.; Ruffino, K.; West, J. Photolithographic Patterning of Polyethylene Glycol Hydrogels. *Biomaterials* **2006**, *27*, 2519–2524.
- (14) Harris, B. P.; Kutty, J. K.; Fritz, E. W.; Webb, C. K.; Burg, K. J. L.; Metters, A. T. Photopatterned Polymer Brushes Promoting Cell Adhesion Gradients. *Langmuir* **2006**, *22*, 4467–4471.
- (15) Khetan, S.; Burdick, J. A. Patterning Hydrogels in Three Dimensions towards Controlling Cellular Interactions. *Soft Matter* **2011**, *7*, 830–838.
- (16) Colak, B.; Di Cio, S.; Gautrot, J. E. Gautrot. Biofunctionalized Patterned Polymer Brushes via Thiol-Ene Coupling for the Control of Cell Adhesion and the Formation of Cell Arrays. *Biomacromolecules* **2018**, *19*, 1445–1455.
- (17) Zahner, D.; Abagat, J.; Frank, S.; Jean, M.; Fréchet, J.; Levkin, P. A. A Facile Approach to Superhydrophilic-Superhydrophobic Patterns in Porous Polymer Films. *Adv. Mater.* **2011**, *23*, 3030–3034.
- (18) Wang, Y.; Lai, H.-H.; Bachman, M.; Sims, C. E.; Li, G. P.; Allbritton, N. L. Covalent Micropatterning of Poly(Dimethylsiloxane) by Photografting through a Mask. *Anal. Chem.* **2005**, *77*, 7539–7546.
- (19) Feng, W.; Li, L.; Ueda, E.; Li, J.; Heißler, S.; Welle, A.; Trapp, O.; Levkin, P. A. Levkin. Surface Patterning via Thiol-Yne Click Chemistry: An Extremely Fast and Versatile Approach to Superhydrophilic-Hydrophobic Micropatterns. *Adv. Mater. Interfaces* **2014**, *1*, 1400269.
- (20) Collins, D. J.; Morahan, B.; Garcia-Bustos, J.; Doerig, C.; Plebanski, M.; Adrian, N. Two-Dimensional Single-Cell Pattering with One Cell per Well Driven by Surface Acounstic Waves. *Nat. Commun.* **2015**, *6*, 8686.
- (21) Ruiz, S. A.; Chen, S. C. Microcontact Printing: A Tool to Pattern. *Soft Matter* **2007**, *3*, 168–177.
- (22) Xu, D.; Bartelt, S. M.; Rasoulinejad, S.; Chen, F.; Wegner, S. V. Green Light Lithography: A General Strategy to Create Active Protein and Cell Micropatterns. *Mater. Horiz.* **2019**, *6*, 1222–1229.
- (23) Yu, Q.; Zhang, Y.; Wang, H.; Brash, J.; Chen, H. Anti-Fouling Bioactive Surfaces. *Acta Biomater.* **2011**, *7*, 1550–1557.
- (24) Agrawal, A.; Luria, E.; Deng, X.; Lahann, J. Landing Rate Measurements to Detect Fibrinogen Adsorption to Non-Fouling Surfaces. J. Cell Mol. Biol. 2012, 5, 320–326.
- (25) Forrest, S. R. The Path to Ubiquitous and Low-Cost Organic Electronic Appliances on Plastic. *Nature* **2004**, *428*, 911–918.
- (26) Xiao, X.; Zimmerman, J. D.; Lassiter, B. E.; Bergemann, K. J.; Forrest, S. R. A Hybrid Planar-Mixed Tetrapheyldibenzoperiflanthene/C70 Photovoltaic Cell. *Appl. Phys. Lett.* **2013**, *102*, 073302.
- (27) Zheng, Y.-q.; Potscavage, W. J.; Komino, T.; Hirade, M.; Adachi, J.; Adachi, C. Highly Efficient Bulk Heterojunction Photovoltaic Cells Cased on C70 and Tetraphenyldibenzoperiflanthene. *Appl. Phys. Lett.* **2013**, *102*, 143304.
- (28) Li, G.; Shinar, J. Combinatorial Fabrication and Studies of Bright White Organic Light-Emitting Devices Based on Emission from Rubrene-Doped 4,4'-Bis(2,2'-Diphenylvinyl)-1,1'-Biphenyl. *Appl. Phys. Lett.* **2003**, 83, 5359.
- (29) Baldo, M. A.; Lamansky, S.; Burrows, P. E.; Thompson, M. E.; Forrest, S. R. Very High-Efficiency Green Organic Light-Emitting Devices Based on Electrophosphorescence. *Appl. Phys. Lett.* **1999**, 75, 4
- (30) He, G.; Schneider, O.; Qin, D.; Zhou, X.; Pfeiffer, M.; Leo, K. Very High-Efficiency and Low Voltage Phosphorescent Organic Light-Emitting Diodes Based on a p-i-n Junction. *J. Appl. Phys.* **2004**, 95, 5773.

- (31) Lahann, J.; Klee, D.; Höcker, H. Chemical Vapor Deposition Polymerization of Substituted [2.2] Paracyclophanes. *Macromol. Rapid Commun.* **1998**, 19, 441–445.
- (32) Lahann, J.; Langer, R. Surface-Initiated Ring Opening Polymerization of -Caprolactone from a Patterned Poly-[(Hydroxymethyl)-p-Xylylene]. *Macromol. Rapid Commun.* **2001**, 22, 968–971.
- (33) Chen, H.-Y.; Lahann, J. Designable Biointerfaces Using Vapor-Based Reactive Polymers. *Langmuir* **2011**, *27*, 34–48.
- (34) McGraw, G. J.; Peters, D. L.; Forrest, S. R. Organic Vapor Jet Printing at Micrometer Resolution Using Microfluidic Nozzle Arrays. *Appl. Phys. Lett.* **2011**, *98*, 013302.
- (35) McGraw, G. J.; Forrest, S. R. Vapor-Phase Microprinting of Multicolor Phosphorescent Organic Light Emitting Device Arrays. *Adv. Mater.* **2013**, 25, 1583–1588.
- (36) S. R., Forrest; G. J., McGraw. Compact Organic Vapor Jet Printing Print Head. US861,349,6B2, 2013.
- (37) Jiang, X.; Chen, H.-Y.; Galvan, G.; Yoshida, M.; Lahann, J. Vapor-Based Initiator Coatings for Atom Transfer Radical Polymerization. *Adv. Funct. Mater.* **2008**, *18*, 27–35.
- (38) Gleason, C. J.; Cox, J. M.; Walton, I. M.; Benedict, J. B. Polymorphism and the Influence of Crystal Structure on the Luminescence of the Opto-Electronic Material 4,4'-Bis(9-Carbazoyl)-Biphenyl. CrystEngComm 2014, 16, 7621–7625.
- (39) Qu, B.; Ding, K.; Sun, K.; Hou, S.; Morris, S.; Shtein, M.; Forrest, S. R. Fast Organic Vapor Phase Deposition of Thin Films in Light-Emitting Diodes. *ACS Nano* **2020**, *14*, 14157–14163.
- (40) MATLAB version 9.7.0, 1434023 (R2019b); The Mathworks Inc., 2019.
- (41) Di Cio, S.; Gautrot, J. E. Gautrot. Cell Sensing of Physical Properties at the Nanoscale: Mechanisms and Control of Cell Adhesion and Phenotype. *Acta Biomater.* **2016**, *30*, 26–48.
- (42) Keselowsky, B. G.; Collard, D. M.; García, A. J. Surface Chemistry Modulates Fibronectin Conformation and Directs Integrin Binding and Specificity to Control Cell Adhesion. *J. Biomed. Mater. Res., Part A* **2003**, *66*, 247–259.
- (43) Faucheux, N.; Schweiss, R.; Lützow, K.; Werner, C.; Groth, T. Self-Assembled Monolayers with Different Terminating Groups as Model Substrates for Cell Adhesion Studies. *Biomaterials* **2004**, 25, 2721–2730
- (44) Schmidt, D. R.; Waldeck, H.; Kao, W. J.. Protein Adsorption to Biomaterials. In *Biological Interactions on Materials Surfaces*; Puleo, D. A., Bizios, R., Eds.; Springer: New York, NY, 2009; pp 1–18.
- (45) Manwaring, M. E.; Walsh, J. F.; Tresco, P. A. Tresco. Contact Guidance Induces Organization of Extracellular Matrix. *Biomaterials* **2004**, 25, 3631–3638.
- (46) Weidt, A.; Mayr, S. G.; Zink, M. Influence of Topographical Cues on Fibronectin Adsorption and Contact Guidance of Fibroblasts on Microgrooved Titanium. *ACS Appl. Bio Mater.* **2019**, *2*, 1066–1077.
- (47) Šafaříková, E.; Šindlerová, L. Š.; Stříteský, S.; Kubala, L.; Vala, M.; Weiter, M.; Víteček, J. Evaluation and Improvement of Organic Semiconductors' Biocompatibility towards Fibroblasts and Cardiomyocytes. Sens. Actuators, B 2018, 260, 418–425.
- (48) Krishna, F.; Lim, R.; Sherwood, C.; Keynes, A.; Brichta, A.; Paul, C. Dastoor. Organic Bioelectronics: Materials and Biocompatibility. *Int. J. Mol. Sci.* **2018**, *19*, 2382.
- (49) Edahiro, J.-i.; Sumaru, K.; Tada, Y.; Ohi, K.; Takagi, T.; Kameda, M.; Shinbo, T.; Kanamori, T.; Yoshimi, Y. In Situ Control of Cell Adhesion Using Photoresponsive Culture Surface. *Biomacromolecules* **2005**, *6*, 970–974.
- (50) Théry, M.; Racine, V.; Pépin, A.; Piel, M.; Chen, Y.; Sibarita, J.-B.; Bornens, M. The Extracellular Matrix Guides the Orientation of the Cell Division Axis. *Nat. Cell Biol.* **2005**, *7*, 947–953.
- (51) Bratton, D.; Yang, D.; Dai, J.; Ober, C. K. Recent Progress in High Resolution Lithography. *Polym. Adv. Technol.* **2006**, *17*, 94–103.
- (\$2) Forrest, S. R. Organic Electronics: Foundations to Applications; Oxford University Press, 2020.

- (53) Shtein, M.; Peumans, P.; Benziger, J. B.; Forrest, S. R. Direct Mask- and Solvent-Free Printing of Molecular Organic Semi-conductors. *Adv. Mater.* **2004**, *16*, 1615–1620.
- (54) Matsushima, T.; Shiomura, K.; Naka, S.; Murata, H. Optical, Morphological, Structural, Electrical, Molecular Orientation, and Electroluminescence Characteristics or Organic Semiconductor Films Prepared at Various Deposition Rates. *Thin Solid Films* **2012**, *520*, 2283–2288.
- (55) Qu, B.; Forrest, S. R. Continuous Roll-to-Roll Fabrication of Organic Photovoltaic Cells via Interconnected High-Vacuum and Low-Pressure Organic Vapor Phase Deposition Systems. *Appl. Phys. Lett.* **2018**, *113*, 053302.
- (56) Søndergaard, R.; Hösel, M.; Angmo, D.; Larsen-Olsen, T. T.; Frederik, C.; Krebs. Roll-to-Roll Fabrication of Polymer Solar Cells. *Mater. Today* **2012**, *15*, 36–49.
- (57) Rivnay, J.; Owens, R. M.; Malliaras, G. G. The Rise of Organic Bioelectronics. *Chem. Mater.* **2013**, *26*, 679–685.
- (58) Liao, C.; Zhang, M.; Yao, M. Y.; Hua, T.; Li, L.; Yan, F. Flexible Organic Electronic in Biology: Materials and Devices. *Adv. Mater.* **2015**, *27*, 7493–7527.
- (59) Cavalcanti-Adam, E. A.; Micoulet, A.; Blümmel, J.; Auernheimer, J.; Kessler, H.; Spatz, J. P. Lateral Spacing of Integrin Ligands Influences Cell Spreading and Focal Adhesion Assembly. *Eur. J. Cell Biol.* **2006**, *85*, 219–224.
- (60) Malmström, J.; Christensen, B.; Jakobsen, H. P.; Lovmand, J.; Foldbjerg, R.; Sørensen, E. S.; Sutherland, D. S. Large Area Protein Patterning Reveals Nanoscale Control of Focal Adhesion Development. *Nano Lett.* **2010**, *10*, 686–694.
- (61) Kim, D. H.; Wirtz, D. Focal Adhesion Size Uniquely Predicts Cell Migration. Faseb. J. 2013, 27, 1351–1361.
- (62) Deshmukh, M. M.; Ralph, D. C.; Thomas, M.; Silcox, J. Nanofabrication Using a Stencil Mask. *Appl. Phys. Lett.* **1999**, 75, 1631.
- (63) Menard, E.; Meitl, M. A.; Sun, Y.; Park, J.-U.; Shir, D. J.-L.; Nam, Y.-S.; Jeon, S.; Rogers, J. A. Micro- and Nanopatterning Techniques for Organic Electronic and Optoelectronic Systems. *Chem. Rev.* **2007**, *107*, 1117–1160.